scientific reports

OPEN

Research on new magnetic epoxy resin composite slurry materials and localization grouting diffusion mechanism

Zhao Li[1,2], Huan Cai[1], Jie Liu[1,2,3]✉, Fan Yu[1], Xiaopeng Bao[1] & Yunan Yang[1,3]

A significant number of steep cracks are frequently encountered in underground engineering, posing a threat to operation. The high-pressure grouting method is a commonly utilized repair technique. Nevertheless, conventional grout is prone to displacement due to its weight, making it challenging to ensure adequate filling of the cracks. Therefore, this study aims to develop a grouting material with targeted displacement and anchoring properties. Firstly, an optimal magnetic slurry composition was determined through an orthogonal test. Subsequently, XRD and SEM were used to analyze the impact of the magnetic field on the composition distribution, internal pore structure, and transient viscosity of the slurry. Afterwards, a model for localized grout diffusion under magnetic was established. The results show that the application of a magnetic field caused the slurry to compact due to magnetic forces, reducing its porosity. Moreover, the dynamic viscosity of the slurry increased exponentially with rising magnetic induction intensity. Notably, a 40.5% increase in the diffusion area was observed when the magnetic field intensity rose from 2500 to 4500 GS. The error between the measured and theoretical values of the magnetic slurry diffusion model was only 8.91%, indicating the model's accuracy in describing the slurry diffusion process under magnetic field influence.

Keywords Fissure plugging, Magnetic epoxy, Magnetic field strength, Viscosity transients, Fixed domain grouting model

With the development and progress of science and technology, the world's transportation, water conservancy, mining and other major infrastructure projects have been rapid development; at the same time, it also brings a lot of construction challenges for the construction of the project, such as underground engineering in the development of dense steeply inclined fissures, high slopes, strong unloading fissure rock grouting reinforcement and other engineering problems, the existing technology is often used in high-pressure grouting method of grouting to fill, but there is still a slurry in the action of the self-gravitation However, there are still problems such as serious loss of slurry under the action of self-weight, small fissure segments are not easy to be filled and compacted, and complicated treatment after grouting, which bring greater harm to the construction and safe operation of the project[1–4]. The complex and changeable grouting environment puts forward higher technical requirements on the performance of slurry materials and grouting process. Therefore, it is particularly important to develop new engineering grouting materials and related processes for rock mass grouting reinforcement management[5–7].

In order to improve the performance of the slurry itself and the retention rate in the fissure, to ensure the quality of grouting. Many scholars have carried out a lot of research work on grouting materials. Kao and Huang et al.[8,9] used Hopkinson rods to carry out dynamical mechanical tests on fissured mudstones reinforced with different slurries, and analyzed the damage morphology and mechanical properties of fissured rocks reinforced with different slurries under impact loading. Peng and Liu et al.[10,11] analyzed the damage morphology and mechanical properties of fissured rocks reinforced with different slurries through the use of 2-aminoethanesulfonic acid (SEA) to hydrophilic modification of epoxy resin (E-44), and studied the effect of modified epoxy resin on the mechanical properties of cement slurry, the results show that modified epoxy resin effectively improves the fracture toughness of the material and increases its ability to resist external impact. Li et al.[12], and Horszczaruk et al.[13]

[1]College of Civil Engineering and Architecture, China Three Gorges University, Yichang 443002, Hubei, China. [2]Key Laboratory of Geological Hazards on Three Gorges Reservoir Area, Ministry of Education, China Three Gorges University, Yichang 443002, Hubei, China. [3]Badong National Observation and Research Station of Geohazards, China University of Geosciences, Wuhan 430074, China. ✉email: 202008140011006@ctgu.edu.cn

used acetone and water as dispersants respectively, and with silica nanospheres doped into the cement to form a composite material, and compared the effect of the two methods on the dispersion of silica nanospheres in the cement and the enhancement of the effectiveness. These modified cement slurries primarily control their specific properties, which could potentially result in the deterioration of other properties. Therefore, many scholars have started to develop new grouting materials with superior performance. These materials are mainly divided into two categories: inorganic grouting materials (such as sodium silicate) and organic grouting materials (such as epoxy resins and polyurethanes). Compared to traditional cement-based materials, they offer advantages such as anti-dispersion, high strength, and good underwater anti-washout performance[14–18]. Colangelo et al.[19], Ai et al.[20], Liu et al.[21], and Yang et al.[22] found that during the grouting process, the bubbles generated by the chemical reaction of the slurry itself and the bubbles that will be introduced under the driving force of the grouting pressure will lead to the existence of a large number of pores in the slurry after consolidation, which are as large as centimeters and as small as nanometers, and the existence of pores weakens the connection of the material and affects the durability and mechanical properties of the material. When the grout is subjected to erosion by harsh substances or when there are changes in the stress of surrounding rocks, the material's porosity will accelerate its tendency to crack, leading to an increased rate of damage and ultimately reducing the material's service life[23–27].

In the field of civil engineering, research on the application of magnetic slurries is still in its exploratory and early development stage. In recent years, some scholars have proposed the concept of magnetically-driven concrete. The principle involves replacing aggregates in concrete with steel slag and using an external magnetic field to control the deviation and movement of the steel slag, thereby achieving the purpose of vibrating the concrete[28–30].Some scholars have also applied electromagnetics to orient the arrangement of steel fibers in steel fiber-reinforced cement-based composite materials to enhance the crack resistance and flexural properties of concrete. Experimental results indicate that the magnetic field has a significant effect on enhancing the strength of steel fiber concrete[31–33]. At present, magnetic slurry is seldom mentioned in the field of rock fissure grouting and repair. In view of the above ideas of adding magnetic substances in engineering materials and the preliminary exploration of magnetic slurry materials, based on the advantages of epoxy resin in the bonding performance and strength enhancement of the slurry[17,33–35], the author has prepared a magnetic slurry material based on the addition of nano-sized magnetic powder particles, fly ash and other additives, which can be oriented to move in fissures and have the magnetic slurry material with fixed-point retention properties is feasible.

In conclusion, significant research achievements have been made in the field of grouting materials and technology. However, there is still room for improvement in terms of grouting material filling density and the effective sealing area of cracks. Based on the advantages of polymers and magnetic adsorption materials, this study developed a novel magnetic epoxy resin composite slurry that demonstrates anti-gravity self-aggregation and adjustable distribution and flow properties under the influence of a magnetic field. Through the magnetic adsorption effect of an external magnetic field, the magnetic slurry is directed to distribute along the magnetic field lines, as illustrated in Fig. 1. The study also investigated the sensitivity of the physical properties parameters of the slurry, as well as the diffusion of grouting filling in micro-pores and cracks, providing a new approach for the development of subsequent grouting materials and grouting technology.

Magnetic slurry materials and test methods

Introduction to the functions of each raw material

To enhance the filling effect of the slurry during cavity crack sealing and improve the retention rate of the slurry in the cracks, this paper proposes a guided magnetic self-aggregating slurry material. Guided by the attraction of magnets to ferromagnetic substances, the slurry is designed to exhibit magnetic self-aggregation and adhesion under the influence of a magnetic field, overcoming its own weight to achieve anti-gravity grouting. The main materials and additives of the magnetic slurry are illustrated in Fig. 2.

(1) Iron(III) oxide powder (Fe_3O_4): Fe_3O_4 iron powder is one of the core materials used in the preparation of magnetic slurry. It has an average particle size of 5–10 μm and a density of 4.8–5.1 g/cm^3. Produced in Shijiazhuang, Hebei, China, the manufacturer is Sunrise Mining Co.

(2) Oil-based epoxy resin: It is a hydrophobic material that provides underwater anti-dispersion properties to the magnetic slurry. The parameters of water-based epoxy resin emulsion and curing agent are shown in Table 1. Manufactured in Guangzhou, China by Guangzhou Kedun Waterproof Material Co.

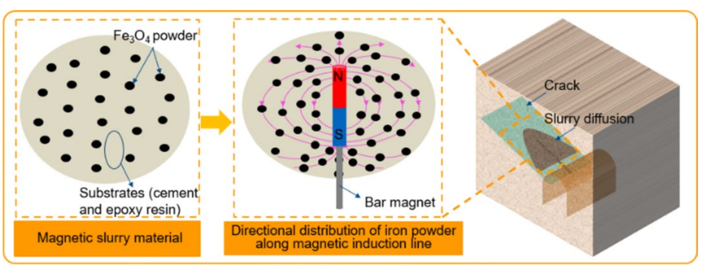

Fig. 1. Principle of crack repair with magnetic slurry.

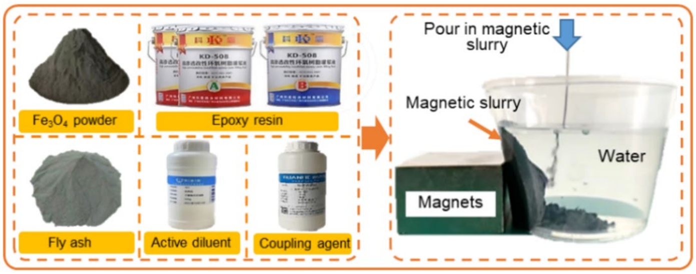

Fig. 2. Composition of magnetic slurry materials.

Product name	Epoxy resin component A	Curing agent component B
Mixing ratio	2	1
Ingredient	C_3H_5CLO, $C_{15}H_{16}O_2$	$C_2H_8N_2$
Density (g/cm^3)	1.16	
Initial viscosity (MPa/s)	190	
Amino value (mg/g)	–	500
Epoxy value	190–210 g/Eq	–

Table 1. Product properties of high-penetration modified epoxy AB grouts.

(3) Fly ash: special fine 800–1250 mesh (10–18 μm) fly ash is used to disperse Fe_3O_4 iron powder particles, reduce the segregation of magnetic field adsorption, and improve the strength of the slurry at the same time. The main chemical components and performance indexes are shown in Table 2. Produced from Shijiazhuang, Hebei, China, the manufacturer was XUYANG MINING INDUSTRY CO.

(4) Reactive diluent: Adopting butyl glycidyl ether as active diluent, adding it to epoxy resin can cross-linking reaction with curing agent, forming a network structure, can effectively enhance the fluidity of epoxy resin. Manufactured by Wuxi Xihua Chemical Technology Co.

Proportion design

Epoxy resin is combined with a specific ratio of high-permeability modified epoxy resin AB grouting slurry (a specialized material for crack repair). Therefore, when designing the mixture, the epoxy resin content is fixed. The performance of the slurry is studied after combining iron powder, fly ash, reactive diluent, and other substances. A three-factor, four-level orthogonal experiment is conducted to analyze the results. The specific proportions are shown in Table 3.

Test methods for magnetic slurry performance on epoxy resin substrates

In order to prepare epoxy resin-based magnetic slurry (ESMS), this paper investigates the influence of three factors on cement-based grouting materials: iron powder, fly ash, and active diluent three kinds of substance doping. The magnetic slurry was prepared according to the following steps and combined with Table 3: (1) Add fly ash, then add magnetic powder, let the two mix well and stir for 60 s; (2) Add oil-based epoxy resin, mix well and stir for 30 s; (3) Add curing agent, mix well and stir for 30 s; (4) Add active diluent, mix well and stir for 20 s; (5) Finally, add coupling agent, mix well and stir for 20 s. The prepared magnetic slurry was subjected to flow test, compressive strength test, setting time test and adsorption performance test, and the trend of the influence of each factor on each performance index was analyzed using the extreme difference method. In addition, the viscosity test was carried out using a digital viscometer, and the microstructure characterization of ESMS was analyzed using XRD and industrial CT. The preparation method and the indoor experimental test method of ESMS are shown in Fig. 3.

Elements	SiO_2	Al_2O_3	CaO	Fe_2O_3	MgO	SO_2	TiO_2	K_2O
Percentage (%)	46.6	33.2	4.2	3.2	1.5	1.28	1.15	0.52

Table 2. Composition and proportion of fly ash components.

S. no.	Epoxy resin A/g	Curing agent B/g	Fe_3O_4 powder/g	Fly ash/g	Reactive diluent/%
1	100	50	40	40	4
2	100	50	40	60	6
3	100	50	40	80	8
4	100	50	40	100	10
5	100	50	60	40	6
6	100	50	60	60	4
7	100	50	60	80	10
8	100	50	60	100	8
9	100	50	80	40	8
10	100	50	80	60	10
11	100	50	80	80	4
12	100	50	80	100	6
13	100	50	100	40	10
14	100	50	100	60	8
15	100	50	100	80	6
16	100	50	100	100	4

Table 3. Orthogonal experiment table for magnetic slurry.

Fig. 3. Magnetic slurry preparation and test methods for indoor experiments.

Experimental setup introduction

To study the diffusion behavior of magnetic fluid in cracks under the influence of magnetic fields, a self-developed visualization grouting test system was established. The experimental system comprises four main components: the crack angle adjustment device, the normal pressure device, data monitoring equipment, and the visualization crack magnetic grouting system. The specific details of the experimental equipment are shown in Fig. 4.

This setup enables real-time imaging of the magnetic grouting process, providing a visual depiction of the infiltration pattern of the fluid and the distribution of the grouting area at various time intervals. During the test, the influence of different magnetic field strengths on the slurry diffusion law under the vertical angle of the fissure was mainly considered, in which: the grouting pressure was 0.6 MPa, and the magnetic induction strengths were set as: 2500GS, 3500GS, and 4500GS, respectively.

Results and discussion

Sensitivity analysis of optimal ratio and parameters of magnetic slurry

Main index of magnetic slurry proportioning

The quality of slurry adsorption is the key to realize the fixed retention of slurry, while the strength of the material is the guarantee of the durability of the grout filling, so the quality of slurry adsorption and the strength after consolidation are used as the first and second main indexes, respectively. As can be seen from Fig. 5, each

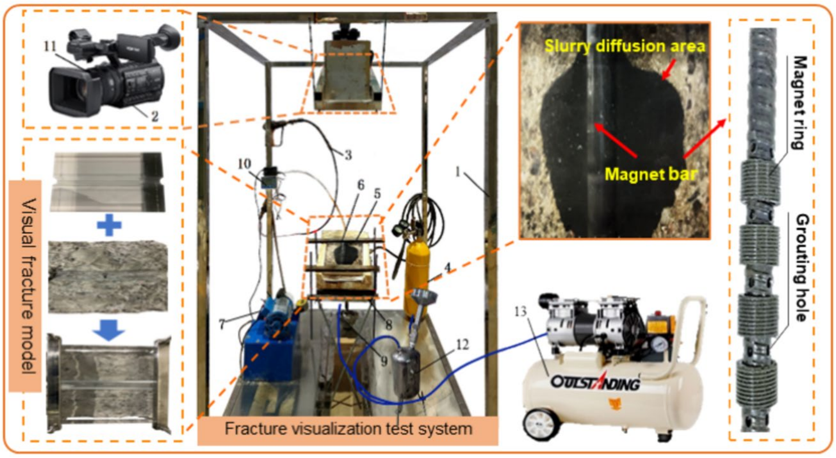

Fig. 4. Visualization grouting test system for cracks. 1—Test stand; 2—HD camera; 3-pipe; 4—High pressure nitrogen bottle; 5—Reaction force frame; 6-visualized magnetic grouting rock sample; 7-dynamic water pressure pump; 8—Pressurized air cushion; 9—Universal ball hinge; 10—Digital flow meter; 11—polarizing mirror; 12-slurry storage tank; 13—Air Compressors.

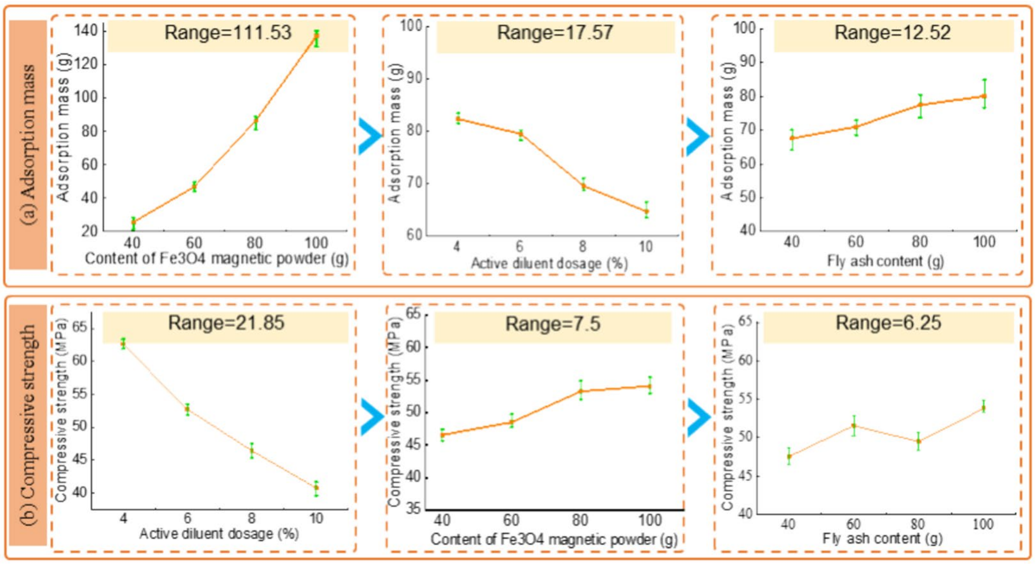

Fig. 5. Polar analysis of the main indicators of magnetic slurry.

factor is analyzed by the extreme difference analysis in the main factor is the same, and the other factors by taking the average value of the R value obtained. Thus the order of significance of the effect on the adsorption quality of the slurry is Fe_3O_4 magnetic powder (R = 111.53) > active diluent (R = 17.57) > fly ash (R = 12.52). The order of effect on compressive strength of the material was active diluent (R = 21.85) > Fe_3O_4 magnetic powder (R = 7.5) > fly ash (R = 6.25).

When the doping amount of Fe_3O_4 magnetic powder is increased from 40 to 100 g, the adsorption mass grows 4.34 times and the growth rate of compressive strength reaches 16.1%. The Fe_3O_4 particles inside the slurry are attracted to each other due to the magnetic field, which drives the matrix liquid and other particles wrapped in the slurry to move to the center of the magnetic field, and the more the magnetic powder is doped, the more the adsorption mass will be.

Active diluent is a secondary factor affecting the quality of slurry adsorption, when the active diluent dosage is increased from 4 to 10%, the adsorption quality decreases by 21.3%; the compressive strength decreases by as much as 34.9%, which is due to the fact that the increase in diluent will lead to a decrease in the cross-linking reaction of the epoxy resin, which weakened the rigid curing lattice structure, leading to the decrease in compressive strength. The decrease in the cross-linking reaction of the epoxy resin causes a decrease in the viscosity of the slurry, which is macroscopically manifested as an increase in the fluidity, thus leading to a decrease in the adsorption capacity of the slurry.

With the increase in the dosage of fly ash has little effect on the growth of the adsorption quality; the effect on the compressive strength of the law is to first improve and then a small decline and finally improve. This is because with the increase in the dosage of fly ash, to a certain extent, hindered the curing reaction of the oil-based epoxy resin, resulting in a decrease in the density of the polymer cross-linking grid, so that the compressive strength is lowered; and with the dosage of a further increase in the system Fe_3O_4 magnetic powder, fly ash constitutes the slurry of the aggregate support structure, increasing the overall densification of the material, so that the compressive strength of the material is increased.

Magnetic slurry proportioning auxiliary indicators
Fluidity is the key index of slurry pumpability, and the speed of solidification time has a greater impact on the progress of the project, so the fluidity and solidification time as the first and second auxiliary indicators, respectively. Analysis of Fig. 6 shows that the ranking analysis of the size of the extreme difference of each factor, the order of influence on the flow of the material is fly ash (R = 127.75) > Fe_3O_4 magnetic powder (R = 124.5) > active diluent (R = 123.5). The order of influence on the gelling time of the material was active diluent (R = 15.6) > Fe_3O_4 magnetic powder (R = 9.2) > fly ash (R = 7.3).

Diluent is an important factor affecting the slurry setting time, with the content of diluent increased from 4 to 10%, the slurry flow grew by 39.1%, the growth rate of the initial setting time was as high as 20.7%. This is because the active diluent is directly involved in the curing reaction of the epoxy resin, which inhibits the contact between the epoxy resin and the curing agent to a certain extent, slowing down the reaction rate and prolonging the initial setting time. When the dosage of Fe_3O_4 magnetic powder was increased from 40 to 100 g, the slurry flow decreased by 28.4%; the initial setting time increased by 11%. Magnetic powder does not have a chemical reaction with epoxy resin, after adding increased solid particle content within the slurry, resulting in an increase in viscosity of the slurry, the fluidity decreased; at the same time, hindering the direct contact between the epoxy resin and curing agent, slowing down the rate of curing reaction, so the gelation time is prolonged. When the dosage of fly ash was elevated from 40 to 100 g, the decrease in slurry fluidity amounted to 29.4%, while the growth rate of initial setting time was 9.2%. Fly ash leads to prolonged setting time for the same reason as magnetic powder. A certain dosage of fly ash can usually be used as an additive to enhance the flowability, however, when the dosage exceeds a certain limit, the flowability enhancement effect will gradually weaken or even decrease due to the increase of the specific surface area of the fly ash and the increase of the amount of water required to be encapsulated.

Comprehensive Figs. 5, 6 analysis results: the most significant impact on the quality of the slurry adsorption for Fe_3O_4 iron powder, with the increase in the content of iron powder was adsorbed slurry quality was a steep increase in the trend of tensile strength of the impact is a slight increase in the amount of active diluent doping on the adsorption amount and tensile strength of the impact of the negative correlation; from the analysis of the fluidity indicators, compared to Fe_3O_4 iron powder doping 40 g, doping of 80 g, fluidity decreased only 4.6%, while doping 100 g, fluidity decreased by 28.4%. From the analysis of flow index, compared with the Fe_3O_4 iron powder dosage of 40 g, the dosage of 80 g only decreased by 4.6%, while the dosage of 100 g decreased by 28.4%. Therefore, the optimal ratio (mass) of the slurry is w(epoxy resin A):w(epoxy resin B):w(Fe_3O_4 iron powder):w(fly ash):w(active diluent) = 2:1:1.6:2:0.18.

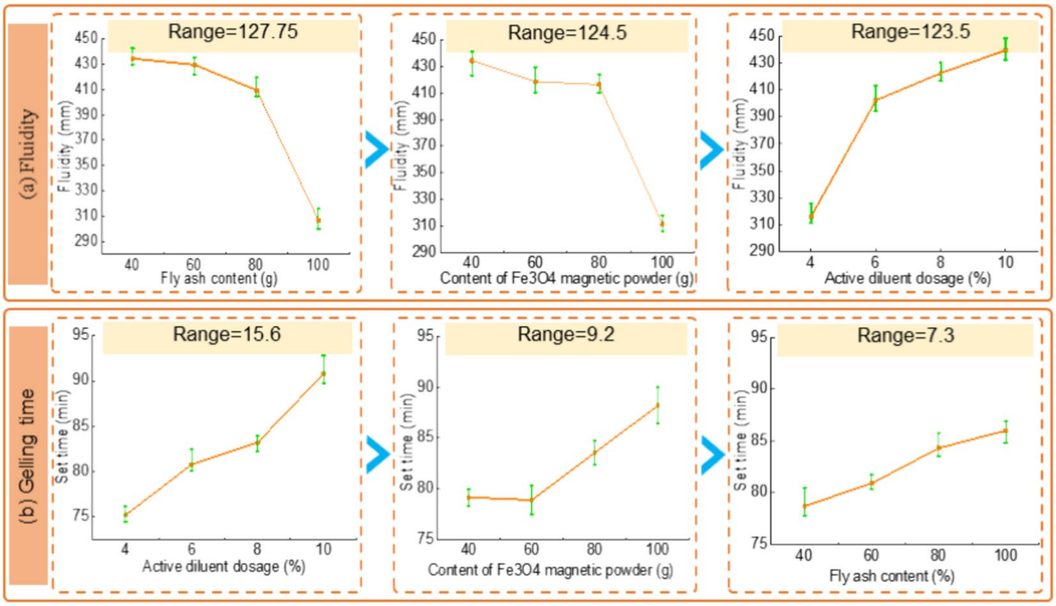

Fig. 6. Polar analysis of magnetic slurry auxiliary indicators.

Analysis of magnetic slurry composition and microscopic pores in different magnetic field regions

Figure 7 shows the composition distribution of magnetic slurry in different magnetic field strength regions. Analyzing Fig. 7a, it can be seen that the strong magnetic field area, the middle magnetic field area and the weak magnetic field area all contain Fe_3O_4, Al_2O_3 and SiO_2 diffraction peaks, and the diffraction peaks of Fe_3O_4 in the strong magnetic field area are higher than those in the middle magnetic field, and the middle magnetic field is higher than that in the weak magnetic field area. This indicates that the magnetic slurry will be attracted to each other due to magnetization, so that part of the Fe_3O_4 particles wrapped in the matrix liquid will move to the strong magnetic field, but the efficiency of the magnetic field area "transferring force" is gradually weakened with the increase of the distance.

Figure 7b and c show the EDS elemental distributions of the specimen A region with and without magnetic field, respectively. It is found that the main elements in the cured products of oil-based epoxy resin are O, Fe, Si, C, etc. Among them, the O element comes from the epoxy resin, the Fe element comes from the applied magnetic powder, and the Ca element comes from the CaO in the fly ash, etc. The weight percentage of the Fe element with magnetic field increased by 1.08% and that of the Ca element increased by 2.85% compared with that without magnetic field. This indicates that under magnetic field, the iron powder in the slurry will converge to the strong magnetic field area, but the degree of segregation is not large, and it is not a single iron powder that generates the movement, but carries the fly ash material along with the movement. This is because the epoxy resin (viscosity value of 0.19 Pa s) in the addition of fly ash viscosity value to the enhancement of the value to 0.45 Pa s, resulting in nanoscale magnetic particles in the slurry by the viscous resistance to a substantial increase in the effect of gravity only, fully stirred magnetic slurry of nanoscale magnetic particles can be dispersed homogeneously, and in the role of the magnetic field also only a small number of Fe_3O_4 particles toward the strong magnetic field area The magnetic particles can be uniformly dispersed in the magnetic slurry after sufficient stirring.

By performing electron microscope scans on specimens cast without a magnetic field and specimens cast with a magnetic field, as shown in Fig. 8, it is observed that the specimen cast without a magnetic field contains numerous pores around 100 μm, whereas the cross-section of the magnetic slurry specimen under a magnetic field appears more compact, with only a few pores around 5 μm.

From the weak magnetic field area to the strong magnetic field area, both the number and the area of pores in the solidified slurry decrease significantly. Compared to the weak magnetic field area, the total pore area decreased by 37.3% in the intermediate magnetic field area and by 87.57% in the strong magnetic field area. Similarly, the number of pores decreased by 34.33% and 78.05% in the intermediate and strong magnetic field areas, respectively. Specifically, the area of large pores (> 0.18 mm) decreased by 37.9% and 87.77%, while the area of medium pores (0.1–0.18 mm) decreased by 27.27% and 81.82% in the intermediate and strong magnetic field areas, respectively. The area of micro-pores in the intermediate and strong magnetic field regions is almost negligible. This indicates that the movement of iron powder has extruded some bubbles while filling the corresponding areas of pores within the magnetic slurry, demonstrating a certain degassing effect.

Analysis of power-viscosity transient effects and spatial distribution of magnetogenic chains in magnetic slurries

Magnetic slurry viscosity transient effects and zoning definition

To analyze the changes in magnetic induction intensity and dynamic viscosity of magnetic slurry at different positions within the magnetic field, a gaussmeter and a rotational viscometer were used to measure the magnetic induction intensity and dynamic viscosity of the slurry in the magnetic field environment, as shown in Figs. 9

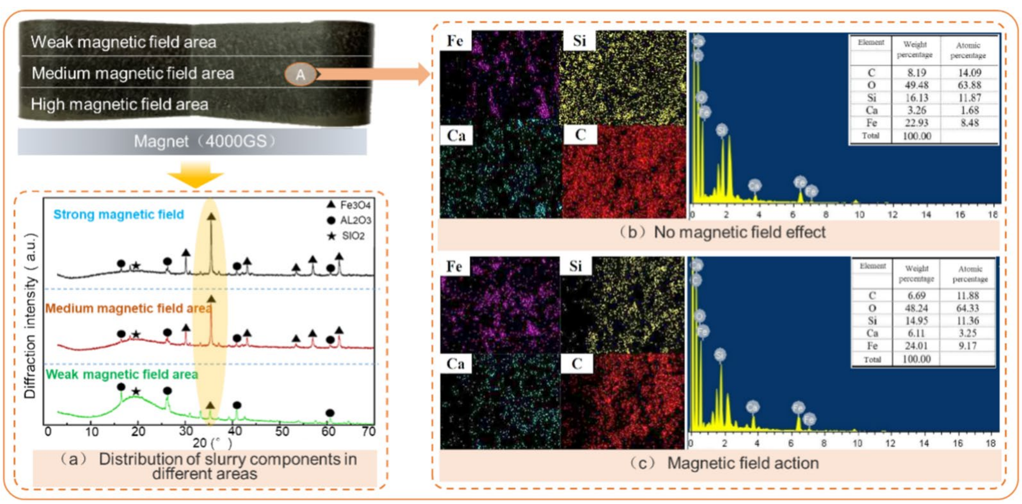

Fig. 7. Distribution of magnetic slurry components in different magnetic field intensity regions.

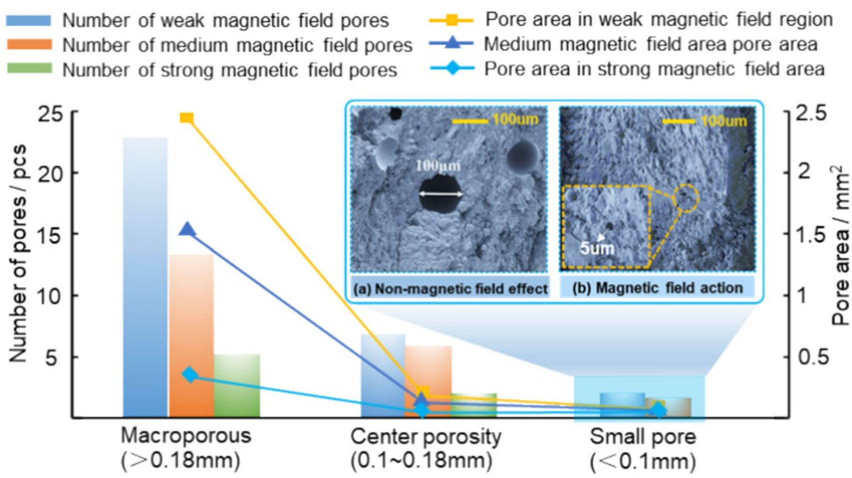

Fig. 8. Distribution of internal pores in magnetic slurry after solidification in different intensity magnetic field regions.

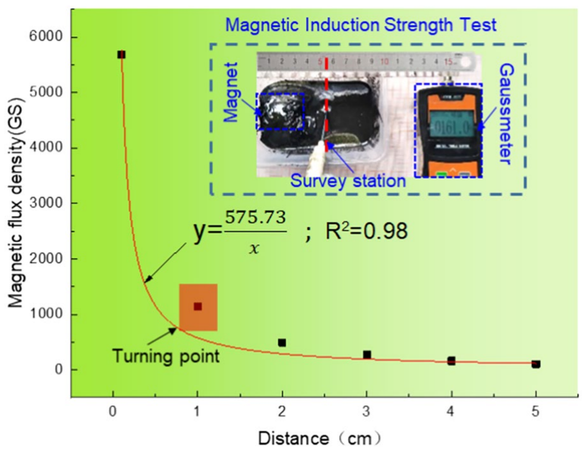

Fig. 9. Variation of magnetic induction in the region of different magnetic fields.

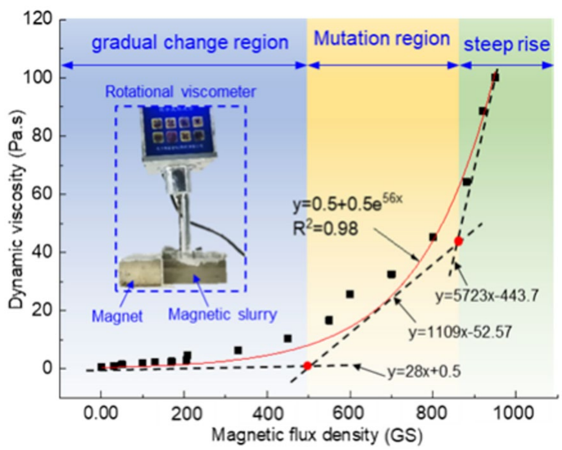

Fig. 10. Illustrates the influence of magnetic induction intensity on dynamic viscosity.

and 10. The initial setting time of the magnetic slurry in air is 30 min, while the viscosity test time is about 1 min, so the viscosity test value of the slurry will not be affected by the long exposure time.

Analyzing Fig. 9, it can be seen that the magnetic induction strength of the magnetic slurry increases with the distance from the measurement point can be better fitted by the inverse proportional function, and the relation is as follows:

magnetic flux density:

$$B = \frac{575.73}{x} \tag{1}$$

where: B is the magnetic induction intensity.

The value of magnetic induction strength at 1 cm from the magnet decreased by 78.95% compared to the magnetic induction strength at the surface of the magnet. Taking 1 cm from the magnet as the inflection point, the magnetic induction strength decreases significantly with increasing distance, indicating that increasing the distance from the measurement point leads to a large attenuation of the magnetic field strength.

Figure 10 shows the effect of magnetic induction strength on the dynamic viscosity, the relationship between the slurry dynamic viscosity and magnetic induction strength can be better fitted with an exponential function, the relationship is as follows:

$$\mu = \mu_0 + \alpha e^{tB} \tag{2}$$

where μ_0—initial dynamic viscosity of the fluid; α—coefficient of influence of dynamic viscosity; t—coefficient of expansion of magnetic induction intensity.

By drawing tangents at the points of minimum curvature radius at both ends and the middle section of the curve, and identifying the intersection of the three tangents as the critical point, the curve can be divided into three stages: the viscosity gradient zone (0 ≤ B < 490GS), the mutation zone (490 ≤ B < 850GS), and the sharp rise zone (B ≥ 850GS). Compared to the average dynamic viscosity in the gradient zone (3.44 Pa.s), the average dynamic viscosity in the mutation zone and sharp rise zone increased by 10.47 times and 24.49 times, respectively. In particular, the maximum viscosity in the gradient zone increased by 21 times compared to the initial dynamic viscosity, while the magnetic induction intensity only increased by 400GS.

Analysis of fixed-domain grouting and spatio–temporal diffusion law of magnetic slurry fissure

To compare the difference in the diffusion of magnetic slurry with and without magnetic field effects in fractures, experiments were conducted in fractures with a 90° inclination angle. During the injection process, the slurry must overcome its own gravity to achieve fracture filling, as illustrated in the figure below. Without the influence of a magnetic field, the behavior of the magnetic slurry is similar to that of ordinary cement slurry. It gradually flows out from the bottom injection orifice under the influence of gravity (Fig. 11a). With the presence of a magnetic field, the magnetic slurry gradually diffuses laterally along the magnetic field lines of the magnetic ring, without flowing away from the lower part of the fracture due to the effect of self-gravity (see Fig. 11b). It can better "stay" within the fracture, achieving the "localized" injection and diffusion for filling the magnetic slurry in the fracture.

Figures 12, 13 and 14 depict the variation of lateral diffusion distance and diffusion area of magnetic slurry with different magnetic field strengths over time.

Under the influence of a magnetic field, both the lateral diffusion distance and diffusion area of the slurry exhibit a power function growth over time. Compared to a magnetic field strength of 2500 GS, the injection time is shortened by 22.7% and 38.2% respectively for magnetic field strengths of 3500 GS and 4500 GS. This indicates that changes in magnetic field strength will affect the time it takes for slurry diffusion to reach a stable state. The reason behind this is that under the influence of a magnetic field, the magnetic slurry rapidly distributes in the direction of the magnetic field lines. With increasing magnetic field strength, the area over which the slurry is directionally distributed increases, reducing the time required for slurry diffusion under injection pressure and thus shortening the time for slurry diffusion to reach a stable state.

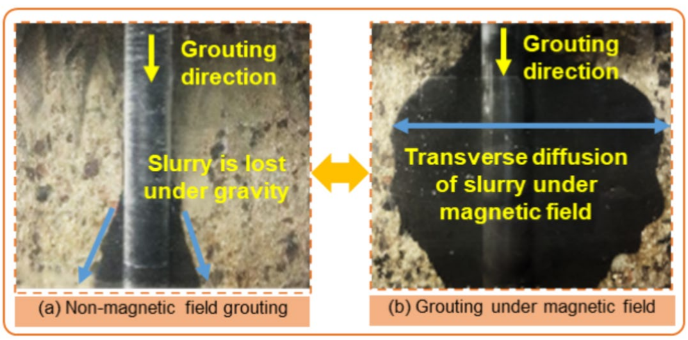

Fig. 11. Vertical fracture injection comparison with and without magnetic field.

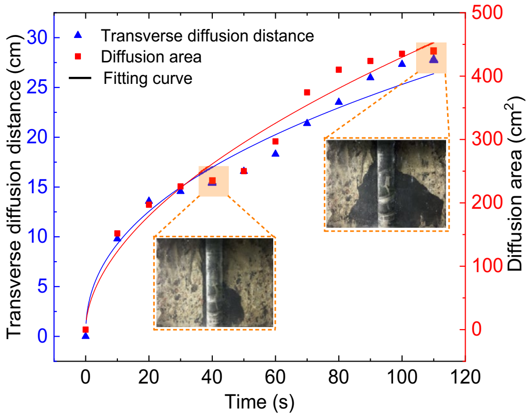

Fig. 12. Variation of lateral diffusion distance and diffusion area over time (2500GS).

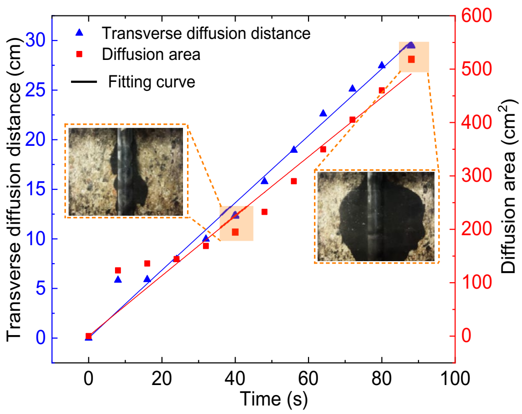

Fig. 13. Variation of lateral diffusion distance and diffusion area over time (3500GS).

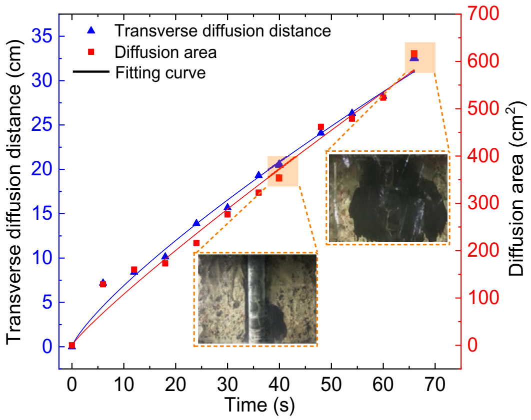

Fig. 14. Variation of lateral diffusion distance and diffusion area over time (4500GS).

Figure 15 illustrates the relationship between the maximum lateral diffusion distance and diffusion area with magnetic field strength.Under the same grouting pressure conditions, when the magnetic induction intensity increases from 2500 to 4500GS, the maximum lateral diffusion distance increases by 16.9%, and the diffusion area increases by 40.5%. This indicates a significant increase in the diffusion area of the slurry with the increase in magnetic field strength. The magnetic field's influence range expands as its strength increases, causing the magnetic slurry to gradually distribute along the shape of the magnetic field lines during diffusion. This oriented distribution provides a localized diffusion area for slurry filling, indicating that the larger the magnetic field intensity, the larger the localized diffusion area. This area obstructs the downward flow of the slurry under gravity,

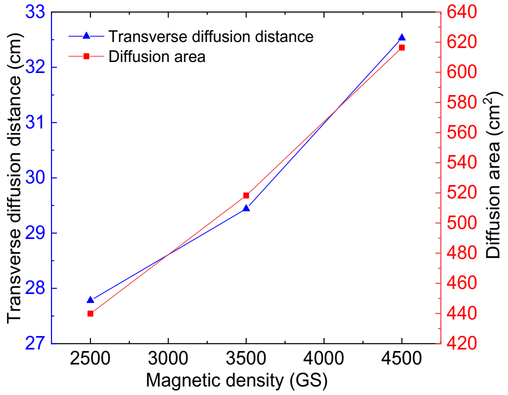

Fig. 15. Relationship between maximum lateral diffusion distance, diffusion area, and magnetic field strength.

leading to the gradual accumulation and outward spread of the slurry based on the localized area. Therefore, under the same grouting pressure conditions, the lower the magnetic field intensity, the smaller the localized diffusion area of the slurry, and the greater influence of gravity on the diffusion area, ultimately resulting in a reduction in the lateral diffusion distance and area of the slurry.

Magnetic slurry fixed-domain grouting diffusion model and validation analysis

Basic assumptions

During the grouting process of magnetic slurry, the viscosity of the slurry changes continuously as it diffuses under the influence of the magnetic field, decreasing gradually as it flows from the grouting orifice to the leading edge of the slurry flow. Based on the following assumptions, the flow control equation of the slurry is established:

The diffusion of the slurry in the fissure is continuous, incompressible, and isotropic fluid.

When the slurry flows on the upper and lower surfaces of the fissure, it satisfies the no-slip condition.

The slurry is in a laminar flow state, satisfying the continuity equation.

Neglect the interaction between the slurry and the surfaces of the fissure.

Constant domain grout diffusion modeling

Based on the above basic assumptions of magnetic slurry fixed-domain grouting diffusion, and combined with the study of magnetic slurry diffusion in vertical fissure under the action of magnetic field, it can be seen that the diffusion morphology is elliptical rather than circular due to the influence of the slurry by magnetic force and gravity effect. Accordingly, a mechanical model of fixed-domain grouting in vertical fissure was established, as shown in Fig. 16.

By introducing Kelvin magnetic force, the magnetofluid dynamics control equation can be described as follows[36]:

$$\frac{\partial (u)}{\partial t} = -\frac{1}{\rho}\nabla p + \mu \nabla^2 u + M \cdot \nabla \mathrm{B} + F \tag{3}$$

here ρ and u denote the density and velocity of the ferromagnetic fluid,μ denotes the kinetic viscosity of the ferromagnetic fluid, p is the pressure, $M \cdot \nabla \mathrm{B}$ denotes the Kelvin magnetic force, t is the time, and F denotes the self-weight of the magnetic slurry.

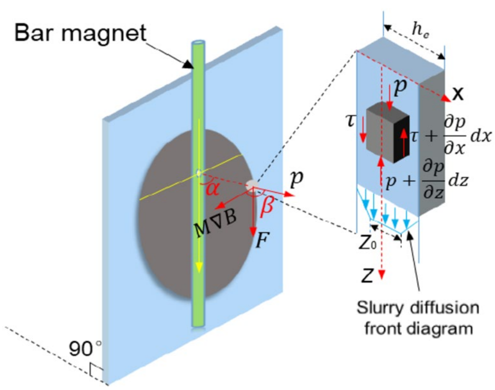

Fig. 16. Vertical crack localized grouting diffusion mechanics model.

Expand the Kelvin magnetic force as follows:

$$(M\cdot\nabla B_x)\overrightarrow{i}=\left(M_x\frac{\partial B_x}{\partial x}+M_y\frac{\partial B_x}{\partial y}+M_z\frac{\partial B_x}{\partial z}\right)\overrightarrow{i} \tag{4}$$

where u, v, w are the velocity components of the slurry in the x, y, z direction respectively.

Substituting Eq. (4) into Eq. (3), the scalar equation of the Navier–Stokes equation for the coupling of magnetic field force and fluid–solid interaction force in the x-direction can be obtained as follows:

$$\frac{\partial u}{\partial t}+u\frac{\partial u}{\partial x}+v\frac{\partial u}{\partial y}+w\frac{\partial u}{\partial z}=-\frac{1}{\rho}\frac{\partial p}{\partial x}+\mu\left(\frac{\partial^2 u}{\partial x^2}+\frac{\partial^2 u}{\partial y^2}+\frac{\partial^2 u}{\partial z^2}\right)+\left(M_x\frac{\partial B_x}{\partial x}+M_y\frac{\partial B_x}{\partial y}+M_z\frac{\partial B_x}{\partial z}\right)+p \tag{5}$$

Considering the assumptions that the diffusion of the slurry in the fissure is continuous, isotropic, and incompressible, and that there is no-slip boundary condition at the upper and lower surfaces of the fissure, then:

$$\frac{\partial \rho}{\partial t}+\nabla\cdot(\rho\boldsymbol{u})=0 \tag{6}$$

$$\frac{\partial v}{\partial y}=0,\frac{\partial w}{\partial z}=0 \tag{7}$$

Combining Eqs. (6) and (7), we can conclude that:

$$\frac{\partial u}{\partial x}=0,\frac{\partial u}{\partial t}=0 \tag{8}$$

The scalar Eq. (5) in the x-direction can be transformed into:

$$\mu\frac{\partial^2 u}{\partial x^2}-\frac{1}{\rho}\frac{\partial p}{\partial x}-M\cdot\nabla B+F=0 \tag{9}$$

Introducing the constitutive equation of Bingham fluid:

$$\tau=\tau_0+\mu\frac{du}{dz} \tag{10}$$

where τ denotes the shear stress distributed along the cross-section of the slurry, τ_0 is the yield shear stress of the slurry.

By analyzing the differential equation of force balance for the unit element, the distribution of sectional shear stress can be obtained:

$$\tau=\begin{cases}0,-\frac{z_0}{2}<z<\frac{z_0}{2}\\ \tau_0,z=\pm\frac{z_0}{2}\\ \frac{2z}{z_0}\tau_0,\frac{z_0}{2}\le|z|\le\frac{h_e}{2}\\ \frac{h_e}{z_0}\tau_0,z=\pm\frac{h_e}{2}\end{cases} \tag{11}$$

By combining Eqs. (10) and (11) and letting" $P=p+\left(M\cdot\nabla B cos\beta-\rho g sin\alpha\right)$" :

$$\frac{d\tau}{dz}=\frac{1}{\rho}\frac{\partial p^*}{\partial x} \tag{12}$$

Integration of Eq. (12):

$$\tau=\frac{1}{\rho}\frac{\partial p^*}{\partial x}z \tag{13}$$

Substituting Eq. (13) into Eq. (10):

$$\frac{du}{dz}=\frac{2z-z_0}{2\rho\mu}\frac{\partial p^*}{\partial x} \tag{14}$$

Integrating Eq. (14) yields the velocity distribution across the section of the slurry:

$$u=\begin{cases}\frac{1}{8\rho\mu}\frac{\partial P}{\partial x}\left(4z^2-4z_0z+2h_ez_0-{h_e}^2\right),\frac{z_0}{2}\le|z|\le\frac{h_e}{2}\\ \frac{1}{4\rho\mu}\frac{\partial p^*}{\partial x}(h_e-z_0)^2,-\frac{z_0}{2}<z<\frac{z_0}{2}\end{cases} \tag{15}$$

The average velocity is:

$$\overline{u}=-\frac{{h_e}^2}{24\rho\mu}\left(\frac{\partial P}{\partial x}-\frac{9\tau_0}{h_e}\right) \tag{16}$$

Flow continuity conditions were used:

$$\overline{u} = \frac{dx}{dt} \tag{17}$$

Based on this, the relationship between the injection time t and the diffusion radius of the slurry as the interface progresses from $x = 0$ to any radius x can be established:

$$\int_0^t \overline{u}dt = \int_0^x dx \tag{18}$$

After rearrangement:

$$\frac{\partial P}{\partial x} = \frac{9\tau_0}{h_e} - \frac{24\rho\mu x}{{h_e}^2 t} \tag{19}$$

Integrating Eq. (19) with respect to x yields:

$$P = \frac{9\tau_0}{h_e}x - \frac{12\rho\mu x^2}{{h_e}^2 t} + p + \left(M \cdot \nabla \text{B}cos\beta - \rho gsin\alpha\right)x \tag{20}$$

When the slurry spreads to the maximum distance $x = R$, $P = 0$. Substituting into Eq. (20), the relationship between the maximum diffusion distance R and time t is obtained as:

$$t = \frac{12\rho\mu R^2}{{h_e}^2\left[p + \left(\frac{9\tau_0}{h_e} + M \cdot \nabla \text{B}cos\beta - \rho gsin\alpha\right)R\right]} \tag{21}$$

Comparative analysis of experimental results and diffusion modeling

To validate the rationality of the diffusion model, the influence of different magnetic field strengths on the slurry diffusion distance was analyzed. The magnetic induction intensity and dynamic viscosity were calculated using Eqs. (1), and (2), respectively. The specific calculation parameter values are shown in Table 4. Substituting the calculated parameters into Eq. (21), the curve of the lateral diffusion distance of the slurry over time under different magnetic field strengths was obtained, as shown in Fig. 17.

Annotation: The saturation magnetization of Fe_3O_4 powder is 60.8 emu/g.

Analyzing Fig. 17, it can be observed that both the theoretical and experimental values of the diffusion distance of the slurry increase non-linearly over time, with the theoretical values consistently exceeding the experimental values.

The lateral diffusion distance of the slurry varies with different magnetic field intensities, gradually increasing as the magnetic field intensity rises, while the time required for grouting significantly decreases. In the early stage of grouting, there is a significant difference between the theoretical and experimental values of the slurry diffusion distance under various magnetic field intensities. When the grouting time is 20 s, the theoretical lateral

$\frac{h_e}{cm}$	$\frac{\tau_0}{kPa}$	Magnetic field strength (GS)	Grouting pressure p (kPa)	Density ρ (kg/m^3)
0.2	0.08	2500/3500/4500	600	1500

Table 4. Calculation parameters.

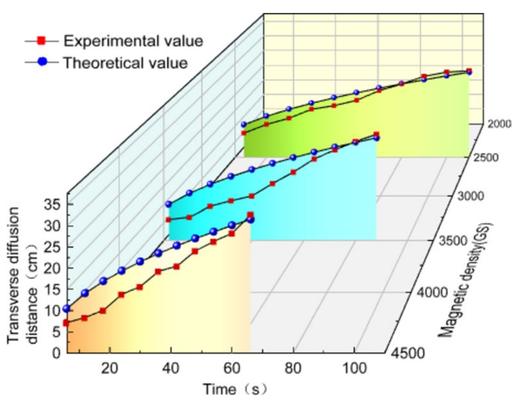

Fig. 17. Relationship between lateral diffusion distance of slurry and time under different magnetic field intensities.

diffusion distances of the slurry corresponding to magnetic field intensities of 2500GS, 3500GS, and 4500GS are 13.18 cm, 15.57 cm, and 16.95 cm, respectively, while the experimental values are 10.58 cm, 9.5 cm, and 10.13 cm, respectively. The maximum relative error between them is 67.3%, and the average relative error is 51.92%. In the later stage of grouting, the relative error between the theoretical and experimental values of the slurry diffusion distance under different magnetic field intensities is relatively small, with a maximum relative error of only 3.17%. The deviation between the theoretical and experimental values is mainly attributed to the roughness of the fissures in the experiment, which was not considered in the theoretical derivation. This discrepancy leads to a situation where the theoretical values exceed the experimental values.

To reduce the error between the theoretical and experimental values of the slurry diffusion distance, define the correction coefficient β as the ratio of experimental value to theoretical value of lateral diffusion distance, and establish the functional relationship between β and time t (as shown in Fig. 18), then we have:

$$\beta = \frac{R}{R_i} = \xi t^{\lambda} = \left\{ \begin{array}{l} 0.51x^{0.15}(2500\text{GS}) \\ 0.13x^{0.46}(3500\text{GS}) \\ 0.33x^{0.25}(4500\text{GS}) \end{array} \right\} \tag{22}$$

where: R—the experimental diffusion distance; R_i—the theoretical diffusion distance. ξ and λ—coefficients influencing the lateral diffusion distance ratio. t—the grouting time.

By introducing the correction coefficient β to modify Eq. (18), we have:

$$t = \frac{12\rho\mu R^2\beta}{{h_e}^2\left[p + \left(\frac{9\tau_0}{h_e} + M\cdot\nabla\text{B}cos\beta - \rho gsin\alpha\right)R\right]} \tag{23}$$

Analyzing Fig. 19, it can be observed that the error between the theoretical and experimental values of slurry diffusion distance under the influence of three different magnetic field intensities is relatively small after adjustment. The maximum relative error is only 8.91% when the grouting time is 66 s under a magnetic field intensity of 4500GS, which is reduced by 86.76% compared to the uncorrected maximum relative error value. This indicates

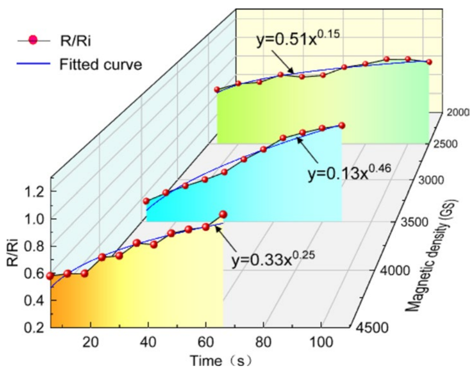

Fig. 18. Relationship between lateral diffusion distance ratio and time.

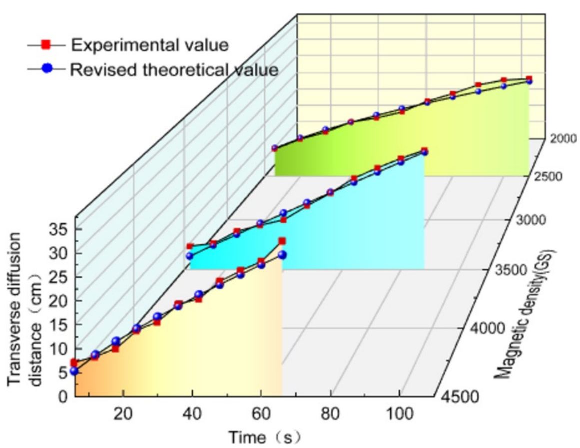

Fig. 19. depicts the relationship between the corrected lateral diffusion distance of the slurry and time.

that the theoretical values calculated by the diffusion model are in good agreement with the experimental results, further verifying the reliability of the diffusion model.

Conclusion

(1) With micron Fe_3O_4, oily epoxy resin, active diluent and fly ash as raw materials, a kind of magnetic grouting material with the characteristics of guided movement and fixed-point retention under the action of magnetic field was prepared. The sensitivity of the physical performance parameters of the magnetic slurry was also analyzed, in which: Fe_3O_4 magnetic powder, active diluent, fly ash and active diluent have the greatest influence on the adsorption quality, compressive strength, fluidity and gelation time of the slurry, respectively.
(2) In the solidified magnetic slurry, the total pore area of the medium magnetic field area and the strong magnetic field area decreased by 37.3% and 87.57%, respectively, when compared to the weak magnetic field area. This suggests that enhancing the magnetic field intensity can significantly enhance the compactness of the magnetic slurry material.
(3) A relationship between slurry dynamic viscosity and magnetic induction intensity is established through the exponential function. Additionally, a method for defining the partition of slurry viscosity transient effect is proposed. It is found that the maximum viscosity of the gradient zone is 21 times higher than the initial dynamic viscosity, suggesting a sharp increase in viscosity when the magnetic field strength reaches a critical value.
(4) When the magnetic induction strength was increased from 2500 to 4500 GS, the slurry diffusion area increased by 40.5%, indicating that the magnetic slurry can be effectively adsorbed and diffused within the range of the magnetic field influence, and the diffusion area increases with the increase of the magnetic field strength. The magnetic slurry fixed-domain grouting diffusion model considering the magnetic field effect and the change of slurry viscosity with magnetic induction strength was established, and the relative errors were less than 8.91% when comparing the experimental results with the calculated values of the theoretical model.

Data availability

All data generated or analysed during this study are included in this published article.

Received: 19 July 2024; Accepted: 26 August 2024
Published online: 29 August 2024

References

1. Li, X. J., Yang, W. M., Wang, L. G. & Butler, I. B. Displacement forecasting method in brittle crack surrounding rock under excavation unloading incorporating opening deformation. *Rock Mech. Rock Eng.* **47**(6), 2211–2223 (2014).
2. Xu, N. W. *et al.* Comprehensive evaluation of excavation-damaged zones in the deep underground caverns of the Houziyan hydropower station, Southwest China. *Bull. Eng. Geol. Environ.* **76**(1), 275–293 (2017).
3. Jiang, Q. *et al.* In situte experimental investigation of basalt spalling in a large underground powerhouse cavern. *Tunn. Undergr. Space Technol.* **68**(1), 82–94 (2017).
4. Zhang, Y. T., Xiao, M. & Chen, J. T. Seismic damage analysis of underground caverns subjected to strong earthquake and assessment of post-earthquake reinforcement effect. *Disaster Adv.* **3**(4), 127–132 (2010).
5. Zhou, Y. Y. *et al.* The failure mechanism and construction practice of large underground caverns in steeply dipping layered rock masses. *Eng. Geol.* **250**, 45–64 (2019).
6. Jiang, Y. F. *et al.* Evolution mechanism of tunnel water and sand inrush considering water-rich sandy dolomite hazard-causing structures. *Eng. Fail. Anal.* **153**, 107554 (2023).
7. Liu, B., Sang, H. M., Wang, Z. Q. & Kang, Y. S. Experimental study on the mechanical properties of rock fracture after grouting reinforcement. *Energies* **13**(18), 4814 (2020).
8. Kao, S. M. *et al.* Dynamic mechanical characteristics of fractured rock reinforced by different grouts. *Adv. Civ. Eng.* https://doi.org/10.1155/2021/8897537 (2021).
9. Ming, H., Xu, C. S., Zhan, J. W. & Wang, J. B. Comparative study on dynamic properties of argillaceous siltstone and its grouting-reinforced body. *Gemech. Eng. A* **13**(2), 333–352 (2017).
10. Peng, Z. G., Zeng, W., Feng, Q. & Zheng, Y. Study on improving the toughness of silicate cement stone by modified epoxy resin. *Silicon* **15**(7), 3137–3148 (2023).
11. Liu, W. T., Sun, Y. D., Meng, X. X. & Qin, Y. Y. Experimental analysis of nano-SiO_2 modified waterborne epoxy resin on the properties and microstructure of cement-based grouting materials. *Energy* **268**, 126669 (2023).
12. Li, H., Yang, H. Q. & Li, X. Y. Investigation on the working performance of a non-dispersible grouting material for the crack repairment of underwater structures. *Constr. Build. Mater.* **2023**, 133558 (2023).
13. Horszczaruk, E. *et al.* Effect of incorporation route on dispersion of mesoporous silica nanospheres in cement mortar. *Constr. Build. Mater.* **66**, 418–421 (2014).
14. Sun, Y. N. *et al.* Grouting material development and dynamic grouting test of broken rock mass. *J. Mater. Civ. Eng.* **34**(5), 1–15 (2022).
15. Liu, X. F., Wang, J. G., Huang, K. & Li, F. Y. Experimental study on dynamic water grouting of modified water-soluble polyurethane. *KSCE J. Civil. Eng.* **23**(9), 3897–3906 (2019).
16. Demir, B. *et al.* A predictive model of interfacial interactions between functionalised carbon fibre surfaces cross-linked with epoxy resin. *Compos. Sci. Technol.* **159**, 127–134 (2018).
17. Tran, N. P., Nguyen, T. N. & Ngo, T. D. The role of organic polymer modifiers in cementitious systems towards durable and resilient infrastructures: a systematic review. *Constr. Build. Mater.* **360**, 129562 (2022).
18. Wu, H., Zhu, M. J., Liu, Z. & Yin, J. Developing a polymer-based crack repairing material using interpenetrate polymer network (IPN) technology. *Constr. Build. Mater.* **84**, 192–200 (2015).

19. Colangelo, F. *et al.* Preparation and characterization of new geopolymer-epoxy resin hybrid mortars. *Materials* **6**(7), 2989–3006 (2013).
20. Ai, D. *et al.* Preparation of waterborne epoxy dispersion and its application in 2K waterborne epoxy coatings. *Prog. Org. Coat.* **136**, 105258 (2019).
21. Liu, X., Wang, J., Huang, K. & Li, F. Experimental study on dynamic water grouting of modified water-soluble polyurethane. *KSCE J. Civ. Eng.* **23**(9), 3897–3906 (2019).
22. Yang, L. *et al.* Experimental study on the grouting diffusion process in fractured sandstone with flowing water based on the low-field nuclear magnetic resonance technique. *Rock Mech. Rock Eng.* **56**(10), 7509–7533 (2023).
23. Xu, C. & Han, L. Formation mechanism of slurry consolidated body in different grouting media under dynamic water conditions by the test-simulation method. *KSCE J. Civ. Eng.* **27**(1), 169–180 (2023).
24. Cao, C., Han, L. & Bu, Y. Epoxy resin water-based modification method. *chem. Tech. Fuels oil.* **59**(2), 290–297 (2023).
25. Li, S. C., Wu, J., Xu, Z. H. & Li, L. P. Unascertained measure model of water and mud inrush risk evaluation in karst tunnels and its engineering application. *KSCE J. Civ. Eng.* **21**(4), 1170–1182 (2017).
26. Faure, P. F., Care, S. & Magat, J. Drying effect on cement paste porosity at early age observed by NMR methods. *Constr. Build. Mater.* **29**, 496–550 (2012).
27. Li, K. P., Yang, T. & Jiang, W. Isogeometric boundary element method for isotropic damage elastic mechanical problems. *Theor. Appl. Fract. Mec.* **124**, 103802 (2023).
28. Villar, V. P., Medina, N. F. & Hernández-Olivares, F. A model about dynamic parameters through magnetic fields during the alignment of steel fibres reinforcing cementitious composites. *Constr. Build. Mater.* **201**, 340–349 (2019).
29. Javahershenas, F., Gilani, M. S. & Hajforoush, M. Effect of magnetic field exposure time on mechanical and microstructure properties of steel fiber-reinforced concrete (SFRC). *J. Build.* **35**, 101975 (2021).
30. Chen, J., Wang, J. & Jin, W. L. Study of magnetically driven concrete. *Constr. Build. Mater.* **121**, 53–59 (2016).
31. Xue, W., Chen, J. & Xie, F. Orientation of steel fibers in magnetically driven concrete and mortar. *Materials* **11**(1), 170 (2018).
32. Kang, D., Moon, D. & Kim, W. Changes in rheological properties of mortars with steel slags and steel fibers by magnetic field. *Materials* **14**(14), 4005 (2021).
33. Zhang, X., Du, M. & Fang, H. Polymer-modified cement mortars: Their enhanced properties, applications, prospects, and challenges. *Constr. Build. Mater.* **299**, 124290 (2021).
34. Tran, N. P., Gunasekara, C. & Law, D. W. Microstructural characterisation of cementitious composite incorporating polymeric fibre: A comprehensive review. *Constr. Build. Mater.* **335**, 127497 (2022).
35. Tran, N. P., Gunasekara, C. & Law, D. W. A critical review on drying shrinkage mitigation strategies in cement-based materials. *J. Build.* **38**, 102210 (2021).
36. Chen, M., Niu, X. & Yu, P. Numerical investigation of magnetic-field induced self-assembly of nonmagnetic particles in magnetic fluids. *J. Fluids Struct.* **97**, 103008 (2020).

Author contributions

Conceptualization, Z.L., J.L. and H.C.; methodology, J.L. and Z.L.; validation, Y.F. and X.P.B.; formal analysis, H.C., Z.L. and X.P.B.; data curation, YN.Y, X.P.B.; writing—review and editing, Z.L., Y.F., H.C. and X.P.B. All authors have read and agreed to the published version of the manuscript.

Funding

This research is supported by the Open Fund of Badong National Observation and Research Station of Geohazards (No. BNORSG202313), the National Natural Science Foundation of China (Grant No.: 52079071), the Key Laboratory of Geological Disasters in the Three Gorges Reservoir Area (Grant No.: 2020KDZ08).

Competing interests

The authors declare no competing interests.

Additional information

Correspondence and requests for materials should be addressed to J.L.